

Received November 27, 2020, accepted December 9, 2020, date of publication December 15, 2020, date of current version December 30, 2020.

Digital Object Identifier 10.1109/ACCESS.2020.3045090

# Design of High Efficiency Controller for Wide Input Range DC-DC Piezoelectric Transformer Converter

SEOK-TEAK YUN<sup>1,2</sup> AND SEUNG-HYUN KONG<sup>3</sup>, (Senior Member, IEEE)

<sup>1</sup>Robotics Programs, Korea Advanced Institute of Science and Technology (KAIST), Daejeon 305-701, South Korea

<sup>2</sup>Division of KOMPSAT-7 Program, Korea Aerospace Research Institute, Daejeon 34133, South Korea

<sup>3</sup>The CCS Graduate School of Green Transportation, KAIST, Daejeon 305-701, South Korea

Corresponding author: Seung-Hyun Kong (skong@kaist.ac.kr)

**ABSTRACT** Owing to the increasing demand for low-power electronic devices, the need for miniaturized, light-weight power supplies with a high power density is growing. A piezoelectric transformer, which is a mechanical resonance-based power transformer, can meet these requirements. However, piezoelectric transformers are based on mechanical resonance, and the resonance characteristics depend on the output current, temperature, and other parameters. Thus, their efficiency may rapidly reduce with changes in the resonance characteristics under specific load and temperature conditions. Therefore, this study proposes a technique that estimating the optimal frequency by using the measurements of the input voltage and current phase difference of the piezoelectric transformer and regulating the output voltage using the duty cycle. Modeling and control system analyses are performed to address the control interference problem caused by the plurality of control variables and control outputs. To demonstrate the proposed technique, a 40 W prototype hardware device is developed. The efficiency improvement is confirmed, and the analysis is validated.

**INDEX TERMS** EDF modeling, phase tracking, piezoelectric transformer converter, two-loop analog controller.


## I. INTRODUCTION

The increasing demand for mobile electronic devices is driving the demand for smaller and thinner electronic devices. In most mobile electronic devices, the largest volume is occupied by the power supply. The magnetic winding transformers and inductors generally used as converters in conventional power supplies usually occupy a larger volume than other parts such as switches and integrated circuits. This makes it difficult to produce smaller and thinner electronic devices. Studies have attempted replacing the magnetic winding transformers with piezoelectric transformers [1]. Piezoelectric transformers are very thin devices that transmit electric energy via mechanical vibration energy, with almost no electromagnetic interference (EMI) or noise. In addition, they are price competitive because they can be easily manufactured, owing to the absence of wires. Moreover, they provide excellent safety because they are nonflammable, and they have universal range of applications because of their

high voltage stepping ratio [2]. However, piezoelectric transformers increase the difficulty in designing driving circuits because their electrical characteristics depend on the load and switching frequency [3], [4].

Generally, piezoelectric transformers can be classified as step-up and step-down transformers [5]. A representative example of the step-up type transformer is the Rosen-type piezoelectric transformer with a longitudinal vibration mode. Step-up transformers are often used as power supplies to drive thin-film liquid crystal backlighting, fluorescent bulb ballasts, and miniaturized anion generators. Such applications make full use of the piezoelectric transformer's ability to easily generate high voltages [6]. Representative examples of step-down transformers include piezoelectric transformers that have a thickness extensional mode, contour vibration mode, or radial vibration mode. These are used as small-sized mobile power suppliers, such as DC converters [7], [8].

Step-down piezoelectric transformers have been widely studied, and they have been developed with various circuit topologies and control techniques [8]–[10]. Most studies have concluded that DC transformers, including

The associate editor coordinating the review of this manuscript and approving it for publication was Nasim Ullah .

piezoelectric-based transformers, need to have a simple circuit structure to take full advantage of their small size, and they should be operated at a frequency with the maximum gain under the maximum load condition to improve efficiency [11], [12].

The piezoelectric transformer used for the analysis and validation of the proposed control technique had a disk shape, as shown in Fig. 1. The piezoelectric transformer was prepared with lead zirconate titanate (PZT), and it comprised a circular one-layer primary electrode in the center and a ring-shaped multilayer secondary electrode on the external rim, which was separated from the primary rim. As mentioned, step-down piezoelectric transformers with a radial vibration mode are often used for DC transformers, and accordingly a disk-shaped PZT-based piezoelectric transformer was used in the present study.

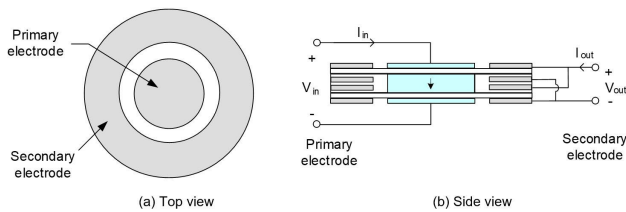


FIGURE 1. Structure of the radial vibration mode disk piezoelectric transformer.

Generally, piezoelectric transformers are coupled field devices that transport energy through an electric/mechanical medium, thus exhibiting electrical characteristics that are different from those of common magnetic transformers [13]. A previous study performed an analysis using an electrical equivalent model to explain the different electrical characteristics related to the design of a DC transformer [14].

In an electrical equivalent model-based analysis, it may be difficult to obtain an accurate analysis and predictions when using mechanical analysis algorithms such as ANSYS and the finite element method (FEM) [15], [16]. Therefore, in the present study, the electrical model parameter values were derived using the piezoelectric transducer model of Mason and KLC [8]. The piezoelectric transformer was converted to a linear model comprising resistances, inductors, and capacitors. The mathematical formula of a determined equivalent model was used to derive the electrical parameter values, which were approximated to the experimental results using the admittance circle method [17], [18].

Fig. 2 shows the electrical equivalent model of a piezoelectric transformer. The  $L_m$ - $C_m$ - $R_m$  resonance part represents the mechanical resonance, and it determines the quality factor ( $Q_m$ ) of the mechanical resonance. Because of the effect of the  $L_m$ - $C_m$ - $R_m$  resonance branch, the piezoelectric transformer is expected to show band-pass filter characteristics [19]. The input side capacitor ( $C_{d1}$ ) and the output side capacitor ( $C_{d2}$ ) represent voltage storage at the input and output electrodes. The voltage storage requires the input and output circuits to be matched for zero voltage switching and output load optimal

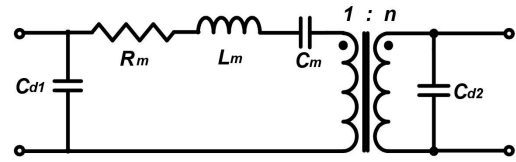


FIGURE 2. Equivalent electrical circuit of the piezoelectric transformer.

design. In addition, the voltage ratio between the primary side and the secondary side can be defined as 1:n.

Table 1 lists the electrical equivalent model parameters that express the characteristics of the piezoelectric transformer in the present study; the values were obtained using the Mason and KLC models and the admittance circle method at room temperature (28°C). The equivalent model shown in Fig. 2 and the parameters listed in Table 1 were used to verify the characteristics of the piezoelectric transformer, subject to variations in the switching frequency, load, and temperature. In addition, the equivalent model and the parameters were used in the control-to-output modeling, the estimation of a high efficiency frequency point, and the controller design.

TABLE 1. Equivalent model parameters at room temperature (28°C).

	Parameter	Value
Resonant branch	$L_m$	16.2 mH
	$C_m$	73.4 pF
	$R_m$	68 ohm
1st stage capacitor	$C_{d1}$	780 pF
2nd stage capacitor	$C_{d2}$	18.9 nF
Voltage stepping ratio	$n$	1 : 0.20

Fig. 3 shows the variation in the voltage gain of the piezoelectric transformer according to the variation in the frequency and load resistance. As shown in Fig. 3, the shape of the voltage gain curve is similar to that of a band-pass filter. In addition, as the load resistance is increased, the frequency

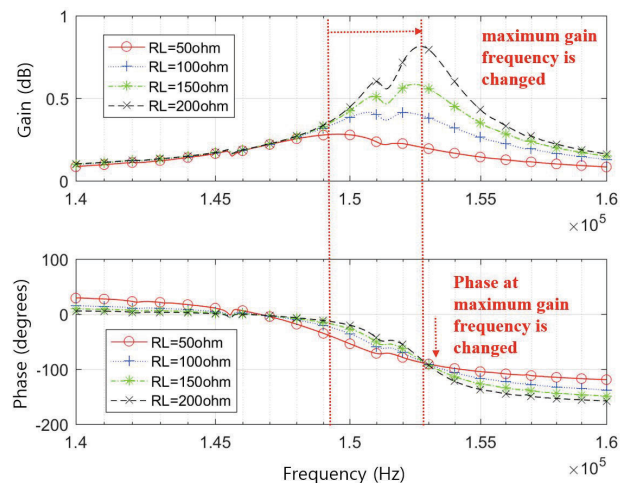


FIGURE 3. Voltage gain characteristics versus frequency and load change (100% to 10%).

of the maximum voltage gain also increased, and the phase changed at the maximum voltage gain frequency [19]. It has been reported that the material constants of the materials used in a piezoelectric transformer change with an increase in the temperature [17]. Accordingly, the parameter values of the electrical equivalent model of a piezoelectric transformer were changed with the temperature. This change in characteristics was investigated in this study by increasing the operating temperature of the piezoelectric transformer from 28°C to 80°C. Table 2 summarizes the changes in the parameters of the equivalent circuit, resulting from the temperature increase, by using the Mason and KLC models and the admittance circle method.

**TABLE 2. Maximum variance in parameters according to temperature change (28°C to 80°C).**

	Parameter	Maximum variance
Resonant branch	$L_m$	0.0028 mH
	$C_m$	0.0035 pF
	$R_m$	0.0041 ohm
1st stage capacitor	$C_{d1}$	0.0036 pF
2nd stage capacitor	$C_{d2}$	0.0038 nF
Voltage stepping ratio	$n$	0

As shown in Table 2, as the temperature increased, the input and output capacitance and the capacitance of the mechanical resonance part also increased; however, the inductance of the mechanical resonance part and the damping resistance decreased. The transformation ratio of the equivalent model did not change with the temperature. Fig. 4 shows the dependence of the voltage gain on the temperature as analyzed from the data in Table 2. While the resonance frequency of the resonance branch did not change significantly with the variation in the  $L_m$  and  $C_m$  values, the maximum gain switching frequency gradually changed with the variation in the secondary capacitor and the resistance of the resonance branch.

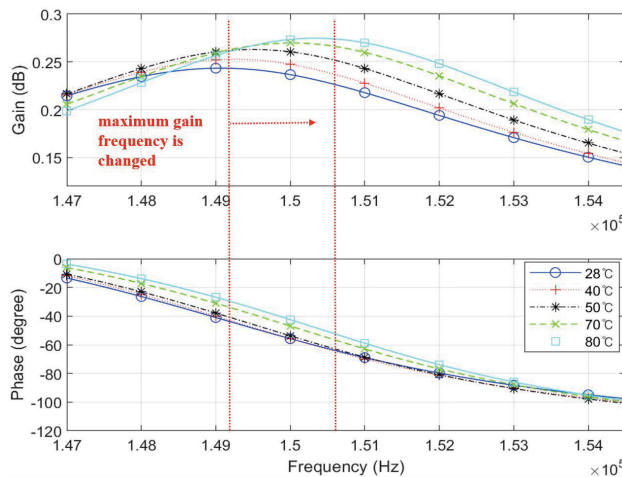


**FIGURE 4. Voltage gain characteristics versus temperature change (28°C to 80°C).**

Two control techniques are usually employed in piezoelectric transformers used for conventional power supplies [8], [9]. The first is pulse frequency modulation (PFM), which is based on the dependence of the voltage gain dependence on the switching frequency. PFM can be easily applied to control the output voltage by varying the switching frequency. However, because the efficiency of a piezoelectric transformer is determined by the switching frequency, PFM may be inappropriate for applications that require wide input voltage and output current ranges.

The other control technique is pulse width modulation (PWM), where the output voltage is controlled by varying the duty cycle at a fixed driving frequency. Since PWM is implemented at a fixed frequency, high efficiency can be maintained despite changes that do not affect the voltage gain, such as changes in the input voltage. However, the efficiency is reduced by factors that affect the voltage gain, such as the temperature and load [13]. In summary, neither of the conventional control techniques can ensure a high efficiency or output voltage control under large changes in the input voltage, output current, and temperature.

To address this and to maximize the energy transfer efficiency of piezoelectric transformers, this paper proposes an optimal efficient frequency and a duty cycle control technique. This technique can ensure the high-efficiency operation of a piezoelectric transformer even under various input voltage, output current, and temperature conditions.

The remainder of this paper is organized as follows. Section 2 proposes an optimal efficient point tracking technique to address the problems introduced in Section 1, and it analyzes the validity of the proposed technique. Section 3 discusses a modeling analysis that is performed to control the double loop proposed in Section 2. In Section 4, the analytical results from Section 3 are applied to the piezoelectric transformer, in order to propose a compensator design for estimating a high efficiency point and the simultaneous control of output voltage. Section 5 describes an efficiency change experiment to validate the proposed technique, modeling, and compensator design. Finally, Section 6 concludes the paper.

## II. PROPOSED TECHNIQUE

As described in Section 1, the maximum efficiency switching frequency of a piezoelectric transformer depends on the temperature and output load. Therefore, a phase and output voltage control algorithm that allows the optimal switching frequency to be estimated is proposed. The algorithm is based on the correlation between the efficiency of the piezoelectric transformer and the minimum reactive power.

The proposed technique consists of a double loop control. The tracking of the optimal switching frequency and the control of the output voltage are performed simultaneously. When the voltage gain characteristics are changed by the load, the switching frequency is changed, which shifts the operating point from Point A to Point B, as shown in Fig. 5. At the same time, the output voltage is controlled by the duty cycle. The output voltage for the duty cycle control can

be easily measured; however, it is difficult to directly measure the optimal efficiency frequency for frequency control. Hence, an algorithm is required to track the optimal efficiency point.

In the present study, the validity of using the input voltage, input current, and output voltage of the piezoelectric transformer as information for tracking the optimal efficiency switching frequency is tested. The analysis was based considering that the efficiency of the piezoelectric transformer is correlated to the reactive power.

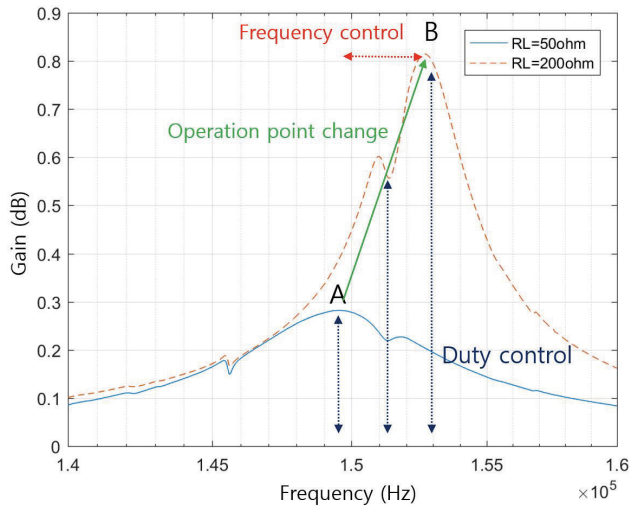


FIGURE 5. Concept of proposed control.

Fig. 6 shows the equivalent circuit of a DC-DC piezoelectric converter, generalized for the analysis. Because of the input capacitor ( $C_{d1}$ ), the input matching circuit is required for high-efficiency operation. Therefore,  $L_a$  and  $L_p$  are used for the generalization of the matching circuit for zero-voltage switching as shown in Fig. 6 [20], [21]. The input voltage,  $v_{AB}$ , can be modeled according to the switch driving circuit [22]. A matching circuit including a direct inductor can be generalized by substituting a large or small  $L_p$ ,  $L_a$  value. In this manner, the equivalent circuit was used to analyze the correlation between the input and the output voltage phase of the piezoelectric transformer, the optimal efficiency frequency, and the correlation between the input impedance and the optimal efficiency frequency.

First, the phase difference of the  $C_{d1}$  voltage and the  $C_{d2}$  voltage is validated to estimate the high efficiency of the piezoelectric transformer. A frequency domain transformation is performed with the components of the piezoelectric transformer shown in Fig. 6. The frequency domain voltage transfer function is expressed as

$$\frac{v_{C_{d2}}(s)}{v_{C_{d1}}(s)} = C_{d2} R_{eq} s \left( \frac{1}{C_m (R_{eq} s + n^2 (1 + C_{d2} R_{eq} s) (1 + C_m (R_m + L_m s) s))} \right), \quad (1)$$

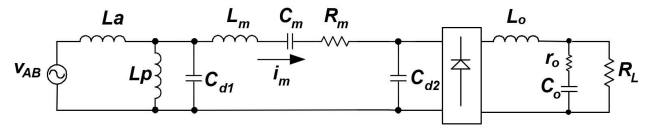


FIGURE 6. General equivalent circuit of the PWM piezoelectric transformer converter.

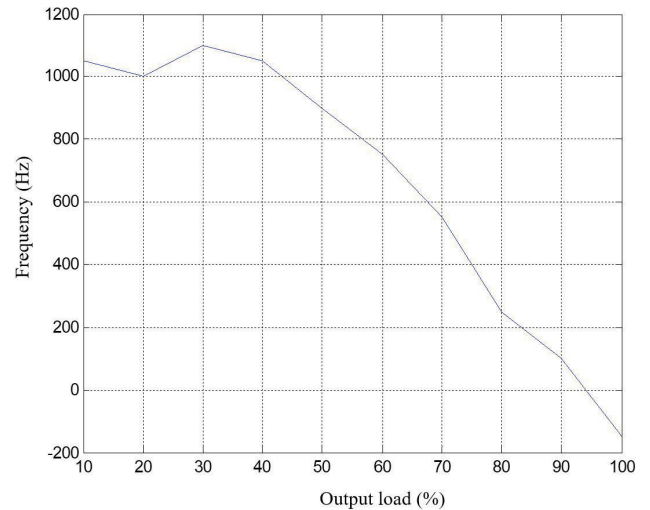


FIGURE 7. Frequency difference between the fixed phase ( $-45^\circ$ ) of a voltage transfer function and the maximum voltage gain frequency with load variation.

where

$$R_{eq} = (\pi^2/2)R_L.$$

Fig. 7 shows the difference between the frequency with the fixed phase ( $-45^\circ$ ) of a voltage transfer function and the maximum voltage gain frequency with load variation. The phase difference of the maximum gain frequency under the maximum load condition is  $-45^\circ$ , therefore this was used for comparison. As shown in Fig. 7, the phase changes at the maximum gain point depending on the load variation. The difference in frequency is up to 1 kHz depending on the load. This makes it difficult to track the optimal efficiency switching frequency by measuring the  $C_{d1}$  voltage and the  $C_{d2}$  voltage without correction.

Next, the correlation between the input impedance phase of the piezoelectric transformer and the optimal efficiency switching frequency is analyzed. The output matching circuit and resistance in Fig. 6 is approximated to  $(\pi^2/2)R_L$ . Hence, the output part of the piezoelectric transformer can be modeled to a direct circuit of  $R'_{eq}$  and  $C'_{d2}$  as

$$R'_{eq}(\omega) = \frac{(\pi^2/2)R_L}{n^2(1 + C_{d2}^2 \cdot ((\pi^2/2)R_L)^2 \cdot \omega^2)}, \quad (2a)$$

$$C'_{d2}(\omega) = \frac{n^2(1 + C_{d2}^2 \cdot ((\pi^2/2)R_L)^2 \cdot \omega^2)}{C_{d2} \cdot ((\pi^2/2)R_L)^2 \cdot \omega}. \quad (2b)$$

The output circuit comprising  $C_{d2}$ ,  $L_o$ ,  $r_o$ ,  $C_o$  and  $R_L$  in Fig. 6 can be converted to a direct circuit by



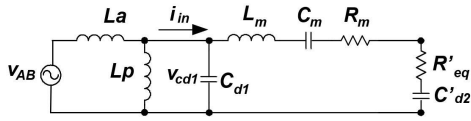


FIGURE 8. Simplified equivalent circuit for input impedance.

using (2a) and (2b), as shown in Fig. 8. The frequency domain input impedance of the piezoelectric transformer can be defined as

$$\frac{X(j\omega)}{1 + j\omega \cdot C_{d1} \cdot X(j\omega)}, \quad (3)$$

where

$$X(j\omega) = (R_m + R'_{eq}(\omega)) + j\omega \cdot (L_m + \frac{C_m \cdot C'_{d2}(\omega)}{C_m + C'_{d2}(\omega)}).$$

Fig. 9 shows the analysis of the difference between the frequency, which causes the reactive component to be zero, and the maximum voltage gain frequency by the load change. As shown in Fig. 9, the maximum error is 90 Hz, which is negligible. Therefore, considering the complications of the system, in the present study, the optimal efficiency switching frequency is estimated by using the phase difference of the input current and input voltage of the piezoelectric transformer.

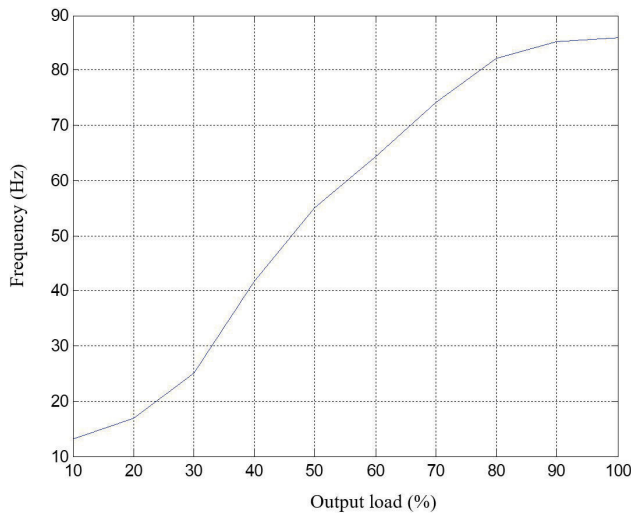


FIGURE 9. Frequency difference between the zero reactive component frequency and maximum gain frequency with load variation.

To address the problems presented in Section 1, we propose the two-loop control for estimating the optimal frequency by using the measurements of the input voltage and current phase difference of the piezoelectric transformer and for regulating the output voltage using the duty cycle.

### III. PIEZOELECTRIC TRANSFORMER CONVERTER MODELING

The optimal frequency estimation and the output voltage control design proposed in Section 2 require the transfer

functions to be modeled for each control. Since the transfer functions of a piezoelectric transformer with band-pass filter characteristics cannot be obtained using general average modeling, the transfer functions are obtained using an extended describing function (EDF), which is a linearization method based on the approximation of the fundamental frequency [22], [23]. It has been reported that the EDF modeling has high accuracy below the switching frequency [24], [25].

First, to obtain the differential equation of the state of the circuit shown in Fig. 6, the state is defined with the  $L_a$  current ( $i_{La}$ ),  $L_p$  current ( $i_{Lp}$ ),  $Cd1$  voltage ( $v_{cd1}$ ),  $Lm$  current ( $i_{Lm}$ ),  $Cm$  voltage ( $v_{cm}$ ),  $Cd2$  voltage ( $v_{cd2}$ ),  $Lo$  current ( $i_{Lo}$ ), and  $Co$  voltage ( $v_{Co}$ ). The input voltage ( $v_{AB}$ ) and output load current ( $i_o$ ) are defined as the input conditions. The state equations for each node are defined as

$$L_a \frac{di_{La}}{dt} = v_{AB} - v_{cd1}, \quad (4a)$$

$$L_p \frac{di_{Lp}}{dt} = v_{cd1}, \quad (4b)$$

$$L_m \frac{di_m}{dt} = v_{cd1} - v_{cm} - v_{cd2} - R_m \cdot i_m, \quad (4c)$$

$$C_{d1} \frac{dv_{cd1}}{dt} = i_{La} - i_m - i_{Lp}, \quad (4d)$$

$$C_m \frac{dv_{cm}}{dt} = i_m, \quad (4e)$$

$$C_{d2} \frac{dv_{cd2}}{dt} = i_m - \text{sign}(v_{cd2}) \cdot i_{Lo}, \quad (4f)$$

$$L_o \frac{di_{Lo}}{dt} = |v_{cd2}| - (1 - \frac{r_o \parallel R_L}{R_L}) \cdot v_{Co} - (r_o \parallel R_L) \cdot (i_{Lo} + i_o), \quad (4g)$$

$$C_o \frac{dv_{Co}}{dt} = \frac{r_o \parallel R_L}{r_o} (i_{Lo} - \frac{v_{Co}}{R_L} + i_o). \quad (4h)$$

In the differential equations above, the nonlinear terms are the input voltage ( $v_{AB}$ ), the sign of  $v_{cd2}$  ( $\text{sign}(v_{cd2})$ ), and the absolute value of  $v_{cd2}$  ( $|v_{cd2}|$ ) [25]. Since the piezoelectric transformer has characteristics similar to a band-pass filter, the voltage created by the switching driving circuit,  $v_{AB}$ , can be represented by a fundamental wave component with a specific frequency.  $\text{sign}(v_{cd2})$  describes the change in  $v_{cd2}$  produced by the effect of the input inductor current on the rectification diode, and  $|v_{cd2}|$  represents the absolute value of the effect of the rectification diode on  $i_o$ . Except  $i_{Lo}$  and  $v_{Co}$ , all the voltage and current states are approximated as fundamental wave components and are simplified with sine envelope terms ( $i_s, v_s$ ) and cosine envelope terms ( $i_c, v_c$ ) by the switching frequency ( $\omega_s$ ) as

$$i(t) \cong i_s(t) \cdot \sin(\omega_s t) + i_c(t) \cdot \cos(\omega_s t), \quad (5a)$$

$$v(t) \cong v_s(t) \cdot \sin(\omega_s t) + v_c(t) \cdot \cos(\omega_s t). \quad (5b)$$

Because the envelope terms have time constants smaller than the switching frequency [22], all the state equations in (4) can be written as

$$\frac{di(t)}{dt} = \left( \frac{di_s(t)}{dt} - \omega_s \cdot i_c(t) \right) \cdot \sin(\omega_s \cdot t)$$

$$+ \left( \frac{di_c(t)}{dt} + \omega_s \cdot i_s(t) \right) \cdot \cos(\omega_s \cdot t), \quad (6a)$$

$$\frac{dv(t)}{dt} = \left( \frac{dv_s(t)}{dt} - \omega_s \cdot v_c(t) \right) \cdot \sin(\omega_s \cdot t)$$

$$+ \left( \frac{dv_c(t)}{dt} + \omega_s \cdot v_s(t) \right) \cdot \cos(\omega_s \cdot t). \quad (6b)$$

All the state equations have been simplified by using the fundamental frequency approximation by using (6a) to (6b). However, the nonlinear terms (the input voltage, sign of  $v_{cd2}$ , and absolute value of  $v_{cd2}$ ) still remain. The  $v_{AB}$  can be approximated as the duty cycle ( $D$ ), fundamental wave components ( $\varpi_s$ ), and input voltage ( $v_g$ ) by using the waveforms as in Fig. 10. The  $\text{sign}(v_{cd2})$  and  $|v_{cd2}|$  can be expressed by the envelope terms of  $v_{cd2}$  and the value of  $i_{Lo}$  as

$$v_{AB} \cong f_1(d, v_g) \cdot \sin(\varpi_s t), \quad (7a)$$

$$\text{sign}(v_{cd2}) \cong \frac{1}{i_{Lo}} \left( f_2(v_{cd2s}, v_{cd2c}, i_{Lo}) \cdot \sin(\omega_s t) + f_3(v_{cd2s}, v_{cd2c}, i_{Lo}) \cdot \cos(\omega_s t) \right), \quad (7b)$$

$$|v_{cd2}| \cong f_4(v_{cd2s}, v_{cd2c}). \quad (7c)$$

In (7), the nonlinear term,  $f_1$ , is defined as a fundamental frequency component of an asymmetric waveform of  $v_{AB}$  by using the Fourier series. The driving circuit used in the present study is analyzed with reference to an asymmetric type PWM-based driver circuit, to maximize the voltage stepping ratio, as shown in Fig. 10. Therefore,  $v_{AB}$  can be modeled with a fundamental component of the switching frequency with a input voltage and duty cycle. In addition, since  $i_{Lo}$  represents the output inductor current, which has a smaller time constant as the switching,  $i_{Lo}$  may be assumed to be DC. Because  $\text{sign}(v_{cd2})i_{Lo}$  is a square wave with the same phase as  $v_{cd2}$ ,  $f_2$  and  $f_3$  may be defined by dividing the fundamental wave components with the absolute value of  $v_{cd2}$  and the fundamental coefficient of the square wave. Finally,  $f_4$  may be approximated as the average of the switching period, as the time constant of the output current is small. Therefore,  $f_1$  to  $f_4$  can be approximated as

$$f_1 \cong \frac{2}{\pi \cdot (1-D)} \cdot \sin(\pi \cdot D) \cdot v_g, \quad (8a)$$

$$f_2 \cong \frac{4}{\pi} \cdot \frac{v_{cd2s}}{\sqrt{v_{cd2s}^2 + v_{cd2c}^2}} \cdot i_{Lo}, \quad (8b)$$

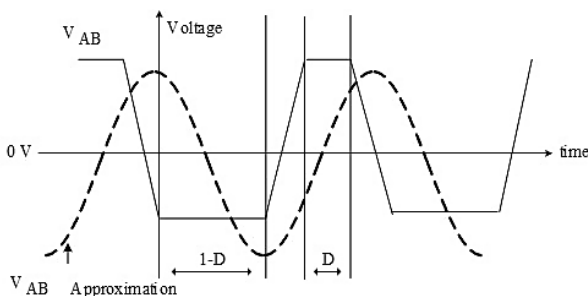


FIGURE 10. Approximation to  $V_{AB}$  waveform.

$$f_3 \cong \frac{4}{\pi} \cdot \frac{v_{cd2c}}{\sqrt{v_{cd2s}^2 + v_{cd2c}^2}} \cdot i_{Lo}, \quad (8c)$$

$$f_4 \cong \frac{2}{\pi} \cdot \sqrt{v_{cd2s}^2 + v_{cd2c}^2}. \quad (8d)$$

By substituting (6), (7), (8) in (4), two differential equations for each state may be obtained, as (9a) to (9n).  $i_{Las}$ ,  $i_{Lac}$ ,  $i_{Lps}$ ,  $i_{Lpc}$ ,  $i_{Lms}$ ,  $i_{Lmc}$ ,  $v_{cd1s}$ ,  $v_{cd1c}$ ,  $v_{cms}$ ,  $v_{cmc}$ ,  $v_{cd2s}$ , and  $v_{cd1c}$  denote the sine and cosine envelope terms of the state at the fundamental frequency.

$$L_a \cdot \left( \frac{di_{Las}}{dt} - \omega_s \cdot i_{Lac} \right) = \frac{2v_g}{\pi(1-D)} \cdot \sin(\pi \cdot D) - v_{cd1s}, \quad (9a)$$

$$L_a \cdot \left( \frac{di_{Lac}}{dt} + \omega_s \cdot i_{Las} \right) = -v_{cd1c}, \quad (9b)$$

$$L_p \cdot \left( \frac{di_{Lps}}{dt} - \omega_s \cdot i_{Lpc} \right) = v_{cd1s}, \quad (9c)$$

$$L_p \cdot \left( \frac{di_{Lpc}}{dt} + \omega_s \cdot i_{Lps} \right) = v_{cd1c}, \quad (9d)$$

$$L_m \cdot \left( \frac{di_{Lms}}{dt} - \omega_s \cdot i_{Lmc} \right) = v_{cd1s} - v_{cms} - v_{cd2s} - r_m \cdot i_{Lms}, \quad (9e)$$

$$L_m \cdot \left( \frac{di_{Lmc}}{dt} + \omega_s \cdot i_{Lms} \right) = v_{cd1c} - v_{cmc} - v_{cd2c} - r_m \cdot i_{Lmc}, \quad (9f)$$

$$C_{d1} \cdot \left( \frac{dv_{cd1s}}{dt} - \omega_s \cdot v_{cd1c} \right) = i_{Las} - i_{Lms} - i_{Lps}, \quad (9g)$$

$$C_{d1} \cdot \left( \frac{dv_{cd1c}}{dt} + \omega_s \cdot v_{cd1s} \right) = i_{Lac} - i_{mc} - i_{Lpc}, \quad (9h)$$

$$C_m \cdot \left( \frac{dv_{cms}}{dt} - \omega_s \cdot v_{cmc} \right) = i_{Lms}, \quad (9i)$$

$$C_m \cdot \left( \frac{dv_{cmc}}{dt} + \omega_s \cdot v_{cms} \right) = i_{Lmc}, \quad (9j)$$

$$C_{d2} \cdot \left( \frac{dv_{cd2s}}{dt} - \omega_s \cdot v_{cd2c} \right) = i_{Lms} - \frac{4}{\pi} \cdot i_{Lo} \cdot \frac{v_{cd2s}}{\sqrt{v_{cd2s}^2 + v_{cd2c}^2}}, \quad (9k)$$

$$C_{d2} \cdot \left( \frac{dv_{cd2c}}{dt} + \omega_s \cdot v_{cd2s} \right) = i_{Lmc} - \frac{4}{\pi} \cdot i_{Lo} \cdot \frac{v_{cd2c}}{\sqrt{v_{cd2s}^2 + v_{cd2c}^2}}, \quad (9l)$$

$$L_o \cdot \frac{di_{Lo}}{dt} = \frac{2}{\pi} \cdot \sqrt{v_{cd2s}^2 + v_{cd2c}^2} - \left( 1 - \frac{r_o \parallel R_L}{R_L} \right) \cdot v_{Co} - r_o \parallel R_L \cdot (i_{Lo} + i_o), \quad (9m)$$

$$C_o \cdot \frac{dv_{Co}}{dt} = \frac{r_o \parallel R_L}{r_o} \times \left( i_{Lo} - \frac{1}{R_L} \cdot v_{Co} + i_o \right). \quad (9n)$$

Thus, (9) can be assumed to be a generalized model of the piezoelectric transformer convertor, and a steady-state analysis can be performed by obtaining the homogenous solutions of the individual differential equations [22]. To verify the DC steady state modeling results, the voltage gain characteristics of the piezoelectric transformer were calculated in accordance with the frequency at 10% load and full load, respectively. Subsequently, these results were compared with the simulation results. Fig.11 shows a comparison between the calculation results and simulation results at 10% load condition. Meanwhile, Fig.12 shows a comparison between the calculation results and simulation results at full load under 28°C and 80°C conditions. Thus, Fig.11 and 12 validate the result of the DC steady state modeling.

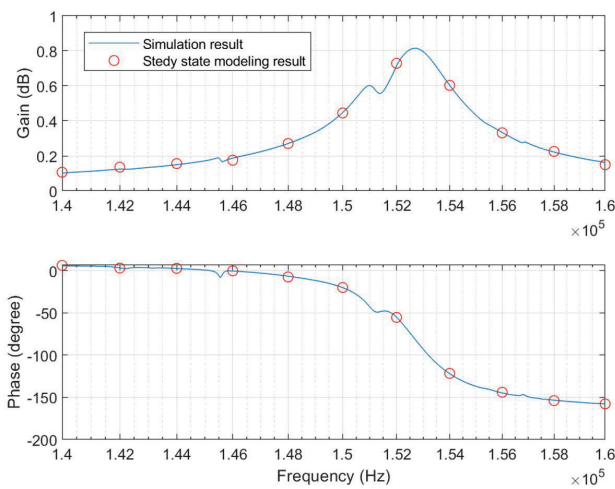


FIGURE 11. Comparison between the calculation results and simulation results at 10% load condition (0.2 A).

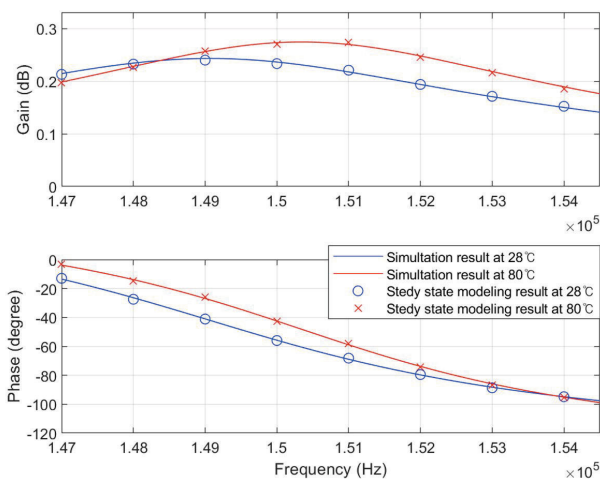


FIGURE 12. Comparison between the calculation results and simulation results at full load (2 A) under 28°C and 80°C conditions.

In addition, the individual envelope terms may be perturbed and linearized for a small-signal analysis, because the time constant is smaller than that of the switching

period [22], [25]. In contrast to the conventional control modeling, the control variables of the proposed two-loop control are the duty cycle and frequency. The output conditions are the input voltage and output current, and the controlled output is the output voltage and input impedance phase. Thus, the proposed technique requires the modeling of the output voltage and the input impedance phase to design the controller. The small signal modeling of the output voltage ( $\hat{v}_o$ ) can be acquired by using the perturbation and fundamental frequency linearization at the  $R_L$  node of the equivalent circuit as

$$\hat{v}_o = r_o \parallel R_L \cdot \hat{i}_{Lo} + \left(1 - \frac{r_o \parallel R_L}{R_L}\right) \cdot \hat{v}_{Co} + r_o \parallel R_L \cdot \hat{i}_o. \quad (10)$$

In contrast, the phase can be modeled by small signal perturbation terms and homogenous solutions at the fundamental frequency. The input current of the piezoelectric transformer,  $i_{in}$ , can be expressed by sine and cosine envelope terms ( $i_{ins}, i_{inc}$ ) as

$$i_{in} = \sqrt{(i_{ins}^2 + i_{inc}^2)} \cdot \sin(\omega_s t - \theta_I). \quad (11)$$

The input current phase steady state ( $\theta_I$ ) and small signal model ( $\hat{\theta}_I$ ) can be defined by homogenous solutions, sine and cosine envelope terms as

$$\theta_I = -\tan^{-1}\left(\frac{i_{inc}}{i_{ins}}\right), \quad (12a)$$

$$\hat{\theta}_I = \frac{I_{inc}}{I_{ins}^2 + I_{inc}^2} \cdot \hat{i}_{ins} - \frac{I_{ins}}{I_{ins}^2 + I_{inc}^2} \cdot \hat{i}_{inc}. \quad (12b)$$

where  $i_{in} = i_{La} - i_{Lp}$ ,  $I_{ins}$ , and  $I_{inc}$  are the homogenous solutions of the input current at the fundamental frequency.

Similar to the input current, the small signal model of the input voltage phase ( $\hat{\theta}_V$ ) can be expressed as

$$\hat{\theta}_V = \frac{V_{cd1c}}{V_{cd1s}^2 + V_{cd1c}^2} \cdot \hat{v}_{cd1s} - \frac{V_{cd1s}}{V_{cd1s}^2 + V_{cd1c}^2} \cdot \hat{v}_{cd1c}. \quad (13)$$

Therefore, the phase difference small signal model of the input current and voltage of the piezoelectric transformer ( $\hat{\theta}$ ) can be expressed as

$$\hat{\theta} = \hat{\theta}_I - \hat{\theta}_V. \quad (14)$$

Fig. 13 shows the diagram of proposed control. The DC input voltage ( $\hat{v}_g$ ) and output currents ( $\hat{i}_o$ ) are defined as the input conditions. In addition, the output voltage ( $\hat{v}_o$ ) and input impedance phase of the piezoelectric transformer ( $\hat{\theta}$ ) are selected as the output variables. The duty cycle ( $\hat{d}$ ) and frequency ( $\hat{f}$ ) are defined as the control variables.

#### IV. HIGH EFFICIENCY TRACKING CONTROLLER DESIGN

Generally, the DC-DC converter control consists of one output variable as it uses one or two control variables [26]–[29]. More specifically, the DC-DC converter employs a voltage

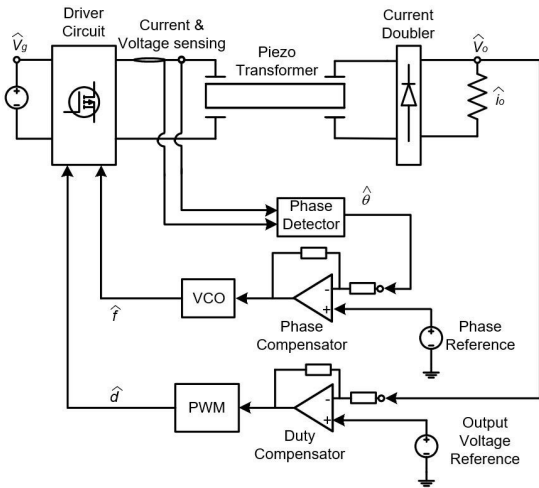


FIGURE 13. Diagram of proposed control.

control in which the output voltage is controlled by being detecting it and using the pulse width or the frequency as a control variable; alternatively, the output voltage is controlled by detecting it and the inductor current and using the duty cycle or the frequency as a control variable [30].

In contrast to the aforementioned control, in the simultaneous voltage and phase control technique proposed herein, two output variables (output voltage and piezoelectric transformer input impedance phase) are controlled simultaneously using two control variables, which are the duty cycle and the switching frequency. Therefore, the stability analysis for the conventional convertor control cannot be applied to the proposed technique.

Accordingly, this section presents the stability and performance analyses of the proposed simultaneous voltage-phase control technique. Fig. 14 presents a diagram of the structure of the pulse width and phase control, where  $G_{vd}$  denotes the transfer function from the duty cycle to the output voltage,  $G_{\theta f}$  denotes the transfer function from the frequency to the input impedance phase of the piezoelectric transformer,  $G_{\theta d}$  denotes the transfer function from the duty cycle to the input impedance phase,  $G_{vg}$  denotes the transfer function from

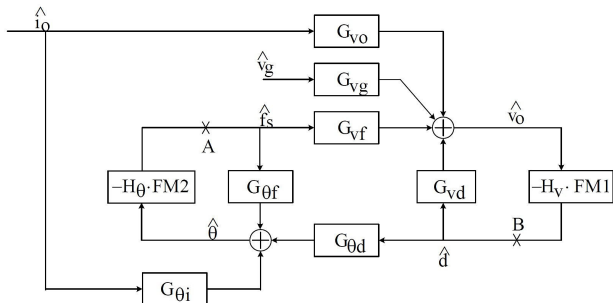


FIGURE 14. Small signal block diagram of the proposed control technique.

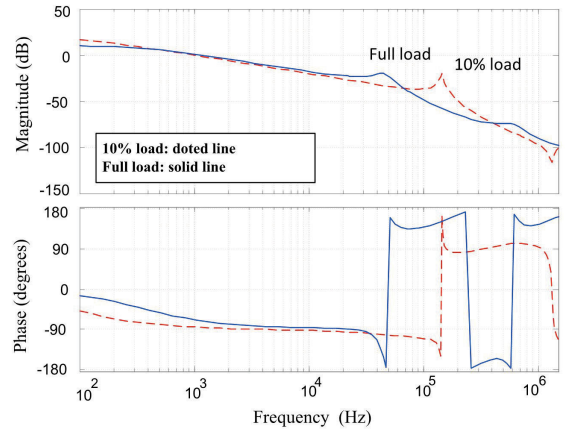


FIGURE 15. Bode plot of duty cycle-to-output voltage ( $G_{vd}$ ) at 100 Vrms under full-load and 10% load conditions.

input voltage to output voltage,  $G_{vo}$  denotes the transfer function from the output current to the output voltage, and  $G_{\theta i}$  denotes the transfer function from the output current to the input impedance phase of the piezoelectric transformer. In addition,  $H_v$  denotes the voltage compensation function, and  $H_{\theta}$  denotes the phase compensation function.

To analyze stability, the loop was opened at Point A in Fig. 14, and the total loop gain value,  $T_{total}$ , was calculated.  $T_{total}$  can be calculated using the input impedance phase loop ( $T_A$ ) and the output voltage loop ( $T_B$ ), as shown in (15a). These loops represent the performance of the output voltage and the phase, respectively. The loop gain,  $T_A$ , can be calculated by obtaining the output of Point A as shown in (15b). The loop gain,  $T_B$ , can be calculated using the same method, as shown in (15c).

$$T_{total} = T_A - \frac{H_{\theta} \cdot FM \cdot H_v \cdot FM1 \cdot G_{vf} \cdot G_{\theta d}}{1 + T_B}, \quad (15a)$$

$$T_A = H_{\theta} \cdot FM2 \cdot G_{\theta f}, \quad (15b)$$

$$T_B = H_v \cdot FM1 \cdot G_{vd}. \quad (15c)$$

$T_{total}$  represents the stability of the entire control system.  $T_A$  mainly has the characteristics of the input impedance phase loop gain, because the output voltage loop affects the phase loop gain adjunctively. Similarly,  $T_B$  mainly has the characteristics of the output voltage loop gain. Therefore, a design that stabilizes both  $T_A$  and  $T_B$  may not ensure the stability of the entire system gain.

To the stabilization design, the worst operating point was derived. Fig. 15 shows  $G_{vd}$  according to the load at 100 Vrms input voltage. As Fig. 15 shows, the phase goes down below  $-180^\circ$  at low frequencies when the load is high. Generally, as the input voltage increases, the gain margin of magnitude decreases [25]. Therefore, the worst operating point was identified as the maximum input voltage (300 Vrms) and full load (2 A) and was used in the analysis in this section.

Fig. 16 shows a Nyquist plot of the total system ( $T_{total}$ ) loop gain at different bandwidth ratio of  $T_A$  and  $T_B$  with a phase margin of  $60^\circ$ . As can be seen from, having a stable  $T_A$  and



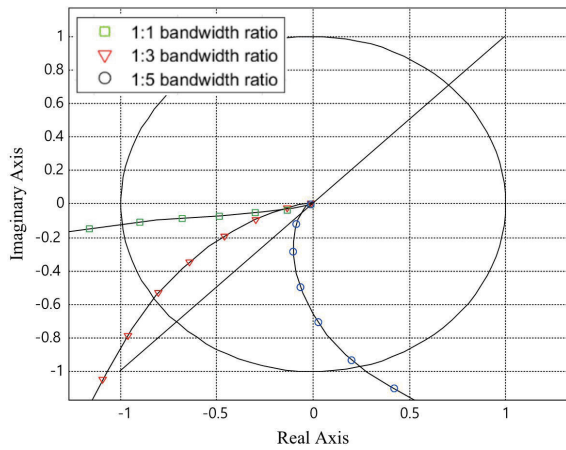


FIGURE 16. Nyquist plot of the total system ( $T_{total}$ ) loop gain at different bandwidth ratio of  $T_A$  and  $T_B$  with same phase margin.

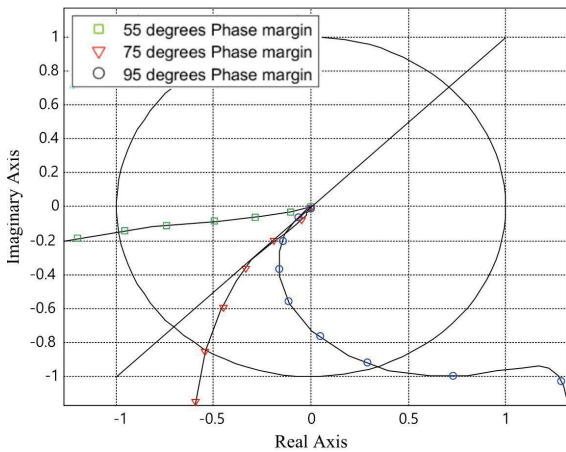


FIGURE 17. Nyquist plot of the total system ( $T_{total}$ ) loop gain at phase margin of  $T_A$  and  $T_B$  with same bandwidth.

$T_B$  does not necessarily mean that the entire system is stable. When the bandwidth ratio of the two loop gains is over 5, the Nyquist plot becomes similar to that of a loop having a large bandwidth; in such a case, it does not compromise the phase margin or stability. Fig. 17 presents a Nyquist plot showing the stability of the entire system when  $T_A$  and  $T_B$  are designed with the same bandwidth (10 kHz) with phase margins of 55°, 75°, and 95°. As Fig. 16 and 17 show, at the bandwidth where  $T_A$  and  $T_B$  are the same, for a stable design, the margin should exceed 75°. However, if the bandwidth ratio exceeds 5, a very high phase margin is not required for each loop. Consequently, for a stabilized design,  $T_A$  and  $T_B$  should have a larger phase margin or the bandwidth ratio between the voltage loop gain and the phase loop gain should be increased.

In this study, the method of increasing the bandwidth ratio of the two loop, which only requires a simple compensator, was selected. As shown in Fig. 18, the compensator of the output voltage loop was designed to have a high bandwidth for rapid regulation of the output voltage. Moreover, as shown

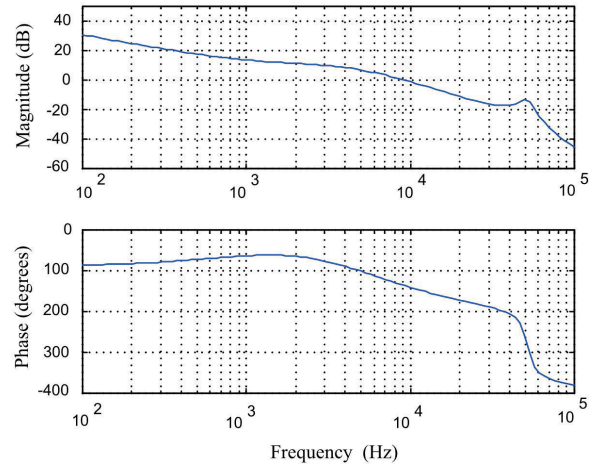


FIGURE 18. Loop gain in point of duty cycle to output voltage view ( $T_B$ ) at worst operation point.

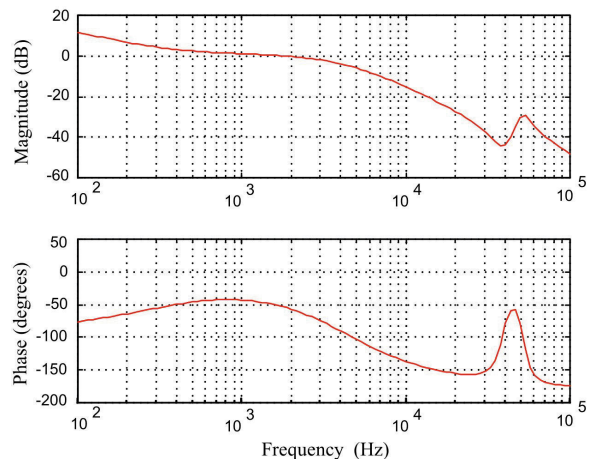


FIGURE 19. Loop gain in point of frequency to input impedance phase view ( $T_A$ ) at worst operation point.

in Fig. 19, the input impedance phase loop was designed to ensure that the bandwidth of the phase loop would be less than 1/5 that of the voltage loop. As a result, the voltage loop was designed to have a bandwidth of 10 kHz and a phase margin of 65° at the worst operating point. While, the phase loop was designed to have a bandwidth of 1 kHz and a phase margin of 50° at the worst operating point. Since the performance of the entire system is determined by controlling the voltage with a large bandwidth, it is expected that  $T_B$  can be used to adjust the output voltage rapidly through disturbances and changes in the operating point, and that  $T_A$  can be used to adjust the input impedance phase more gradually.

## V. EXPERIMENTAL RESULT

This section presents experimental results obtained for an active clamp prototype converter having an output voltage of 20 V and a power of 40 W, to validate the stability, predicted operation, and efficiency of the designed controller. Fig. 20 shows the active clamp prototype converter used

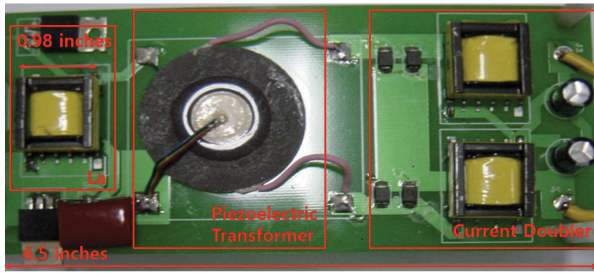


FIGURE 20. The 40 W active clamp prototype converter.

in the experiment. For the sake of simple implementation, a matching circuit in the form of a series inductor ( $L_a$ ) was used in this study. The  $L_a$  was set at  $0.45\text{ mH}$  in the expected switching frequency range (140-160 kHz) of the piezoelectric transformer to ensure that the input impedance would be inductive under both the minimum (0.2 A) and maximum (2 A) loads. In addition,  $220\text{ }\mu\text{F}$  for  $C_o$  and  $300\text{ }\mu\text{H}$  for  $L_o$  were selected.

First, to validate the mathematical small-signal model presented in Section 3, the control-to-output functions were measured and compared using a network analyzer. Fig. 21 shows the open-loop transfer function for output voltage depending on the duty cycle under full-load conditions (2A), with a 150 kHz switching frequency and a 100 Vrms input voltage. Fig. 22 shows the result of the open-loop transfer function of the input impedance phase depending on the frequency under the same conditions. As can be seen from Fig. 21, an error is generated as the frequency is increased. However, below the switching frequency, the results are almost identical. Moreover, the cutoff frequency of the voltage loop transfer function, including the compensator presented in Section 4, is 10 kHz at worst operation point, which is considerably lower than the switching frequency. Similarly, as shown in Fig.22, within 20 kHz, the open loop transfer

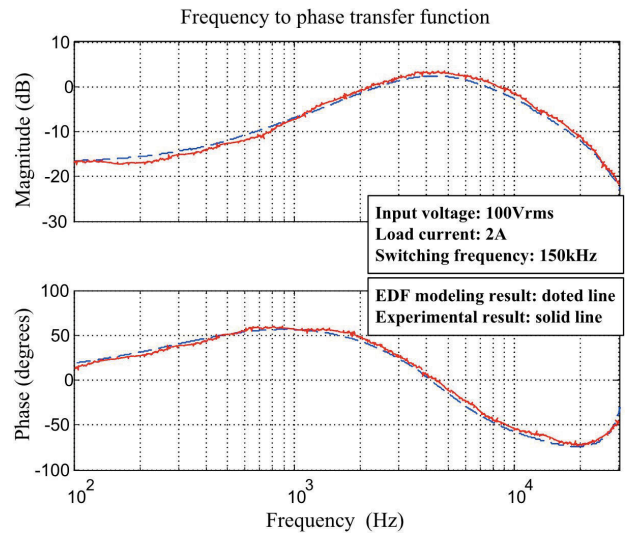


FIGURE 22. The small signal modeling and experiment result for frequency to input impedance phase at full load condition.

function of the phase result is almost identical while the cutoff frequency of the phase-loop transfer function, including for the compensator, is 1 kHz at worst operation point. Therefore, it can be confirmed that the small-signal modeling and compensator design presented in Sections 3 and 4 are suitable for the design of the proposed controller.

Next, to verify control stability, the output load was changed in steps from 10% load (0.2 A) to full load (2 A) under maximum input voltage. Temperature changes enable verification of the stabilization performance of the optimum driving frequency control of the piezoelectric transformer. As the temperature change occurs at a slower rate than that of the load change, variation in the step load becomes the worst condition in the proposed control technique. Therefore, in this paper, the stabilization performance of the controller was verified by measuring the change in the maximum step load.

Fig. 23 shows the waveform of the output voltage depending on the variation in the output current. Point A in Fig. 23 represents operation under a load of 0.2 A, and the duty cycle, switching frequency, input voltage, and input current of the piezoelectric transformer in that interval is shown in Fig. 24. Fig. 25 shows the duty cycle, switching frequency, input voltage, and input current of the piezoelectric transformer waveform at Point B in Fig. 23 under a load of 2 A. As can be seen from Fig. 23, the output voltage remained stable under the maximum load as well as under light loads. In addition, even with a transient interval and load variation, as predicted in Section 4, the variation in the output voltage within the load change duration was only approximately 3 V because of the sufficient margin of the output voltage loop. The experimental results show that the switching frequency and duty cycle at Point A were 154 kHz and 0.2, respectively and that those at Point B were 150 kHz and 0.7, respectively. The phase difference between the input voltage and current of

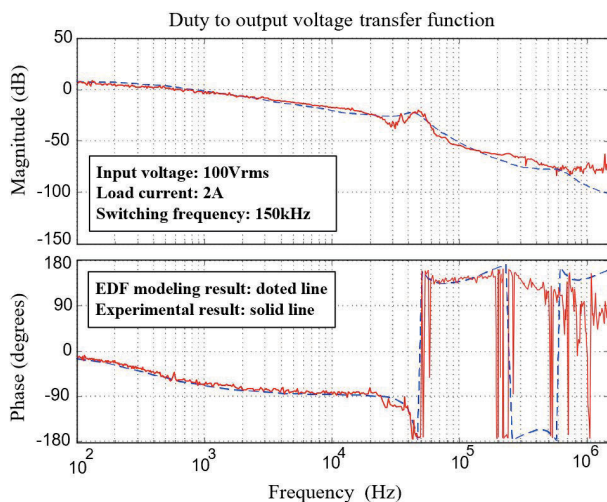


FIGURE 21. The small signal modeling and experiment result for duty cycle to output voltage at full load condition.

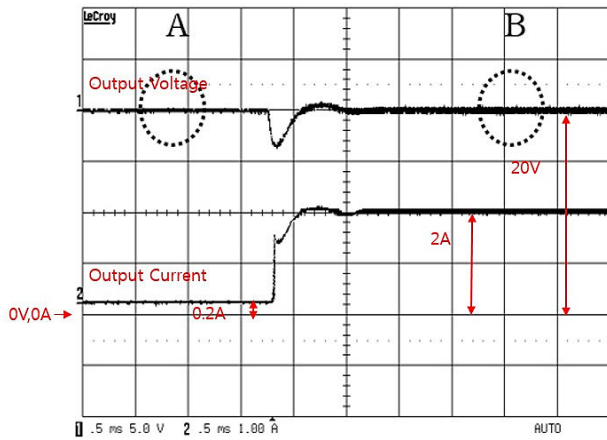


FIGURE 23. Transient response during load variation (0.2 A to 2 A).

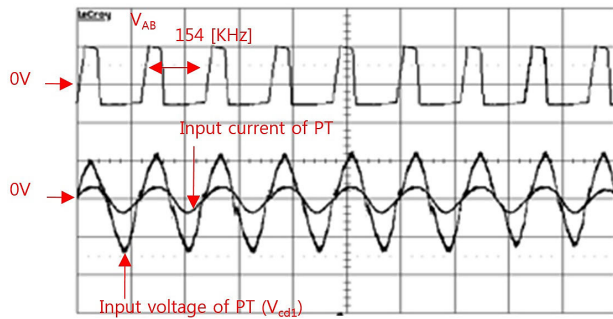


FIGURE 24. Input current, voltage waveform and duty cycle waveforms at 0.2 A load condition.

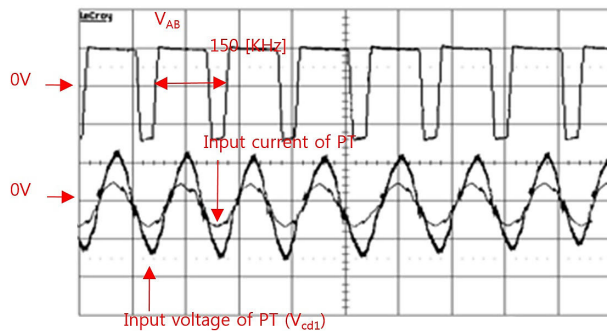


FIGURE 25. Input current, voltage waveform and duty cycle waveforms at 2 A load condition.

the piezoelectric transformer at Points A and B were close to zero, as predicted. Therefore, the stability of the control, modeling, and controller design was verified even under stepped changes in load.

Fig. 26 compares the efficiency of the proposed approach over the entire load range with that of conventional controls. As predicted in Section 2, as the change in voltage depends on the load variation, the PWM-based control enables output voltage control only for a load variation of about 60%. Moreover, while the PFM-based control enables output voltage control depending on load variation, it does not allow

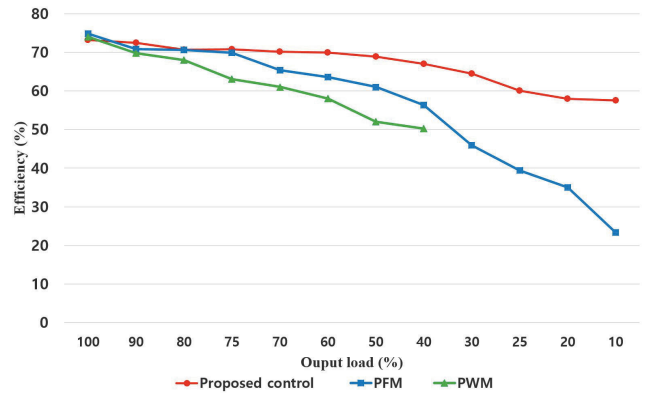


FIGURE 26. Comparison of the efficiency of the piezoelectric transformer converter with load change (100% to 10%).

operation at the maximum-efficiency point, resulting in a continuous reduction in efficiency with varying loads. In contrast, the proposed phase and duty cycle control technique prevents a rapid decrease in efficiency under varying loads, by ensuring the switching frequency corresponding to the optimal efficiency. As can be seen from Fig. 26, with a decrease in load, the efficiency decreased for all the control methods. This may be because of the significant effect of parasitic components and switching losses, which are unavoidable under low loads in a transformer.

Fig. 27 shows the efficiency depending on the variation in input voltage ( $V_g$ ). As can be seen, when the input voltage changed, the efficiency decreased more rapidly in the PFM-based control than in the PWM-based control and the proposed control. More than 72% efficiency was achieved over the entire input voltage range in the PWM-based control and the proposed control.

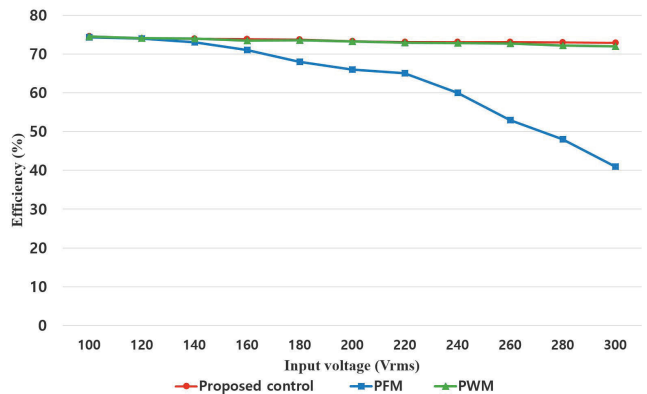


FIGURE 27. Comparison of the efficiency of the piezoelectric transformer converter with input voltage change (100 Vrms to 300 Vrms).

Therefore, the results of the stepped load change experiment validated the stability of the proposed technique. Furthermore, the performance improvement achieved using the proposed technique was verified by measuring the



efficiencies of the different control techniques under varying input voltage and output load.

## VI. CONCLUSION

This paper proposed a technique for estimating the maximum-efficiency point and achieving simultaneous control of the input impedance phase and output voltage of a DC-DC piezoelectric transformer converter. Modeling and analysis of the control system were performed to fully utilize the resonance effect of the piezoelectric transformer.

In the proposed technique, the phase difference between the voltage applied to a resonance circuit and the input current of the piezoelectric transformer is measured to track the optimal-efficiency switching frequency, and the output voltage is simultaneously controlled through the duty cycle. This enables optimal switching frequency operation under various load and temperature conditions.

In addition, to solve the control interference problem when the control involves multiple variables and outputs, modeling, analysis, and compensator design were performed. The results from the system modeling were compared with experimental results to confirm the validity of the system.

A system modeling analysis revealed that the voltage loop controls the output voltage and that the phase loop controls the phase difference. Moreover, a compensator design was developed through modeling. It was confirmed that the system is unstable due to the interaction between the two loops. To address this, a guideline for achieving a stable system design was derived by analyzing the components of the characteristic loop gains of the system. Finally, a 40 W prototype hardware device was developed to demonstrate the stability of the modeling and the improvement achieved using the proposed technique. The results show that the proposed control technique can maximize energy transfer efficiency by effectively compensating for the limitations of a piezoelectric transformer converter.

As the purpose of the prototype transformer in this study is to verify the validity of the proposed control technology, we did not optimize the matching circuit under the proposed technology. Moreover, to verify the control performance under the worst condition, we did not perform a long-term trend experiment in accordance with the temperature change. Therefore, in the future, we aim to optimize the input matching circuits under the optimal frequency driving condition and conduct a long-term trend experiment in accordance with the temperature change.

## REFERENCES

- [1] A. V. Carazo, "Piezoelectric transformers: An historical review," *Actuators*, vol. 5, no. 2, pp. 1–22, 2016.
- [2] C.-Y. Lin and F. C. Lee, "Design and analysis of piezoelectric transformer converter," Ph.D. dissertation, Virginia Tech., Blacksburg, VA, USA, 1997.
- [3] S. Kawashima, O. Ohnishi, H. Hakamata, S. Tagami, A. Fukuoka, T. Inoue, and S. Hirose, "Third order longitudinal mode piezoelectric ceramic transformer and its application to high-voltage power inverter," in *Proc. IEEE Ultrason. Symp. (ULTSYM)*, Cannes, France, 1994, pp. 525–530.
- [4] G. Ivensky, I. Zafrany, and S. Ben-Yaakov, "Generic operational characteristics of piezoelectric transformers," *IEEE Trans. Power Electron.*, vol. 17, no. 6, pp. 1049–1057, Nov. 2002.
- [5] M. Shoyama, K. Horikoshi, T. Ninomiya, T. Zaitzu, and Y. Sasaki, "Operation analysis of the push-pull piezoelectric inverter," in *Proc. Appl. Power Electron. Conf. (APEC)*, Atlanta, GA, USA, Feb. 1997, pp. 573–578.
- [6] O. Ohnishi, H. Kishie, A. Iwamoto, Y. Sasaki, T. Zaitzu, and T. Inoue, "Piezoelectric ceramic transformer operating in thickness extensional vibration mode for power supply," in *Proc. IEEE Ultrason. Symp.*, Tucson, AZ, USA, Oct. 1992, pp. 483–488.
- [7] T. Zaitzu, O. Ohnishi, T. Inoue, M. Shoyama, T. Ninomiya, F. C. Lee, and G. C. Hua, "Piezoelectric transformer operating in thickness extensional vibration and its application to switching converter," in *Proc. Power Electron. Spec. Conf. (PESC)*, Taipei, Taiwan, Jun. 1994, pp. 585–589.
- [8] T. Kim, S. Choi, S. Lee, and B. H. Cho, "New piezoelectric transformer adapter with universal input voltage range," in *Proc. Int. Conf. Power Electron. Drives Syst.*, Kuala Lumpur, Malaysia, 2005, pp. 1223–1227.
- [9] S. Hamamura, D. Kurose, T. Ninomiya, and M. Yamamoto, "New control method of piezoelectric transformer converter by PWM and PFM for wide range of input voltage," in *Proc. 7th IEEE Int. Power Electron. Congr. Tech.*, Acapulco, Mexico, Oct. 2000, pp. 3–8.
- [10] J. A. Martin-Ramos, M. A. J. Prieto, F. N. Garcia, J. D. Gonzalez, and F. M. F. Linera, "A new full-protected control mode to drive piezoelectric transformers in DC-DC converters," *IEEE Trans. Power Electron.*, vol. 17, no. 6, pp. 1096–1103, Nov. 2002.
- [11] M. Sanz, P. Alou, A. Soto, R. Prieto, J. A. Cobos, and J. Uceda, "Magnetic-less converter based on piezoelectric transformers for step-down DC/DC and low power application," in *Proc. 18th Annu. IEEE Appl. Power Electron. Conf. Expo. (APEC)*, Miami Beach, FL, USA, Feb. 2003, pp. 615–621.
- [12] L. Costanzo, A. Lo Schiavo, and M. Vitelli, "Power maximization from resonant electromagnetic vibration harvesters feeding bridge rectifiers," *Int. J. Circuit Theory Appl.*, vol. 47, no. 1, pp. 87–102, Oct. 2018.
- [13] A. M. Flynn and S. R. Sanders, "Fundamental limits on energy transfer and circuit considerations for piezoelectric transformers," *IEEE Trans. Power Electron.*, vol. 17, no. 1, pp. 8–14, Jan. 2002.
- [14] Y. Jin, C. F. Foo, and W. G. Zhu, "Three-dimensional simulation of piezoelectric transformer for the switching power supply," in *Proc. 25th Annu. Conf. IEEE Ind. Electron. Soc. (IECON)*, San Jose, CA, USA, 1999, pp. 295–299.
- [15] C. Y. Lin and F. C. Lee, "Design of a piezoelectric transformer converter and its matching networks," in *Proc. Power Electron. Spec. Conf. (PESC)*, Taipei, Taiwan, 1994, pp. 607–612.
- [16] G. Ivensky, S. Bronstein, and S. Ben-Yaakov, "A comparison of piezoelectric transformer AC/DC converters with current doubler and voltage doubler rectifiers," *IEEE Trans. Power Electron.*, vol. 19, no. 6, pp. 1446–1453, Nov. 2004.
- [17] S. Sherrit, G. Yang, H. D. Weiderick, and B. K. Mukherjee, "Temperature dependence of the dielectric, elastic and piezoelectric material constants of lead zirconate titanate ceramics," in *Proc. Int. Conf. Smart Mater. Struct. Syst.*, Jul. 1999, pp. 121–126.
- [18] S. Bronstein, G. Ivensky, and S. Ben-Yaakov, "Parallel connection of piezoelectric transformers," in *Proc. IEEE 35th Annu. Power Electron. Spec. Conf.*, Aachen, Germany, Jun. 2004, pp. 1779–1785.
- [19] Y.-P. Liu, D. Vasic, F. Costa, W.-J. Wu, and C.-K. Lee, "Design of fixed frequency controlled radial-mode stacked disk-type piezoelectric transformers for DC/DC converter applications," *Smart Mater. Struct.*, vol. 18, no. 8, Aug. 2009, Art. no. 085025.
- [20] S. Bronstein and S. Ben-Yaakov, "Design considerations for achieving ZVS in a half bridge inverter that drives a piezoelectric transformer with no series inductor," in *Proc. IEEE 33rd Annu. IEEE Power Electron. Spec. Conf.*, Cairns, QLD, Australia, Jun. 2002, pp. 585–590.
- [21] M. Ekhtiari, Z. Zhang, and M. A. E. Andersen, "Analysis of bidirectional piezoelectric-based converters for zero-voltage switching operation," *IEEE Trans. Power Electron.*, vol. 32, no. 1, pp. 866–877, Jan. 2017.
- [22] E. X. Yang, F. C. Lee, and M. M. Jovanovic, "Small-signal modeling of series and parallel resonant converters," in *Proc. 7th Annu. Appl. Power Electron. Conf. Expo. (APEC)*, Boston, MA, USA, 1992, pp. 785–792.
- [23] J. A. Martin-Ramos, J. Diaz, A. M. Pernia, M. J. Prieto, and F. F. Linera, "Modelling of the PRC-LCC resonant topology with a capacitor as output filter using EDF," in *Proc. IEEE 33rd Annu. IEEE Power Electron. Spec. Conf.*, Cairns, QLD, Australia, Jun. 2002, pp. 1337–1342.



- [24] E. X. Yang, F. C. Lee, and M. M. Jovanovic, "Small-signal modeling of LCC resonant converter," in *Proc. Rec. 23rd Annu. IEEE Power Electron. Spec. Conf. (PESC)*, Toledo, Spain, 1992, pp. 941–948.
- [25] E. X. Yang, B. Choi, F. C. Lee, and B. H. Cho, "Dynamic analysis and control design of LCC resonant converter," in *Proc. Rec. 23rd Annu. IEEE Power Electron. Spec. Conf. (PESC)*, Toledo, Spain, 1992, pp. 362–369.
- [26] J.-L. Lin and H.-Y. Hsieh, "Dynamics analysis and controller synthesis for zero-voltage-transition PWM power converters," *IEEE Trans. Power Electron.*, vol. 15, no. 2, pp. 205–214, Mar. 2000.
- [27] H. Ma, R. van der Zee, and B. Nauta, "A high-voltage class-D power amplifier with switching frequency regulation for improved high-efficiency output power range," *IEEE J. Solid-State Circuits*, vol. 50, no. 6, pp. 1451–1462, Jun. 2015.
- [28] T. LaBella and J. Lai, "A hybrid resonant converter utilizing a bidirectional GaN AC switch for high-efficiency PV applications," *IEEE Trans. Ind. Appl.*, vol. 50, no. 5, pp. 33468–33475, Sep./Oct. 2014.
- [29] K. Colak, E. Asa, M. Bojarski, D. Czarkowski, and O. C. Onar, "A novel phase-shift control of semibridgeless active rectifier for wireless power transfer," *IEEE Trans. Power Electron.*, vol. 30, no. 11, pp. 6288–6297, Nov. 2015.
- [30] J. L. Sosa, M. Castilla, J. Miret, L. Garcia de Vicuna, and J. Matas, "Modeling and performance analysis of the DC/DC series-parallel resonant converter operating with discrete self-sustained phase-shift modulation technique," *IEEE Trans. Ind. Electron.*, vol. 56, no. 3, pp. 697–705, Mar. 2009.



interests include batteries, power control systems, satellite missions, and fault management operation.

**SEOK-TEAK YUN** received the B.S. degree in electrical engineering from Postech, Pohang, South Korea, in 2005, and the M.S. degree in electrical engineering and computer science from Seoul National University, in 2007. He is currently pursuing the Ph.D. degree in robotics from the Korea Advanced Institute of Science and Technology (KAIST). He joined the Korea Aerospace Research Institute (KARI), in 2007. He is also a Senior Researcher with KARI. His main research



**SEUNG-HYUN KONG** (Senior Member, IEEE) received the B.S. degree in electronics engineering from Sogang University, Seoul, South Korea, in 1992, the M.S. degree in electrical and computer engineering from Polytechnic University (merged to NYU), New York, in 1994, and the Ph.D. degree in aeronautics and astronautics from Stanford University, Palo Alto, in 2005. He is currently an Associate Professor with the CCS Graduate School of Green Transportation, Korea Advanced Institute of

Science and Technology (KAIST), where he has been a faculty member, since 2010. From 1997 to 2004 and from 2006 to 2010, he was with companies including Samsung Electronics (Telecommunication Research Center), Korea, and Qualcomm (Corporate Research and Development Department), San Diego, USA, for advanced technology Research and Development in mobile communication systems, wireless positioning, and assisted GNSS. Since he joined KAIST as a faculty member in 2010, he has been working on various Research and Development projects in advanced intelligent transportation systems, such as robust GNSS-based navigation for urban environment, deep learning and reinforcement learning algorithms for autonomous vehicles, sensor fusion, and vehicular communication systems (V2X). He has authored more than 100 papers in peer-reviewed journals and conference proceedings and 12 patents, and his research group won the President Award (of Korea) in the 2018 international student autonomous driving competition host by the Korean government. He has served as an Associate Editor of IEEE T-ITS and IEEE ACCESS, an Editor of IET-RSN, and the Lead Guest Editor of the IEEE T-ITS Special Issue on "ITS empowered by AI technologie" and the IEEE Access Special Section on "GNSS, Localization, and Navigation Technologies". He has served as the Program Chair of IPNT, from 2017 to 2019, South Korea, and as a Program Co-Chair of IEEE ITSC2019, New Zealand.

...